Uncertainties in sea surface temperature retrievals from space: Comparison of microwave and infrared observations from TRMM

Lucrezia Ricciardulli and Frank J. Wentz
Remote Sensing Systems, Santa Rosa, California, USA

Received 15 December 2003; revised 4 August 2004; accepted 7 October 2004; published 9 December 2004.

[1] A study of the uncertainties in infrared (IR) and microwave (MW) sea surface temperature (SST) retrievals by satellite is described here. The availability of both infrared (VIRS) and microwave (TMI) sensors on the Tropical Rainfall Measurement Mission (TRMM) provided an opportunity to perform this detailed SST intercomparison from two distinct but colocated sensors. Infrared retrievals provide good spatial resolution, but they are limited to clear-sky conditions. Microwave observations provide supplemental SST information in cloudy areas, but they are subject to other limitations such as poor spatial resolution and possible wind biases. One year of colocated VIRS and TMI SSTs are analyzed here, together with other colocated ancillary data sets including surface winds and water vapor, and potential sources of error are presented. The analysis shows some residual IR SST's dependence on atmospheric water vapor, despite corrective terms in the algorithm, with biases of a few tenths of a degree. The inclusion of a water vapor term in the IR algorithm reduces these biases. The results also show a higher uncertainty in MW SST retrievals for winds greater than 12 m/s, and a warm bias of MW SSTs of the order of 1°C within 50–100 km from land. Other potential sources of uncertainties discussed in the paper are undetected clouds, choice of IR SST algorithm, diurnal warming of the skin layer, and satellite maneuvers. The results of this intercomparison are valuable for the development of a future generation of a blended IR/MW SST data set, which combines the strengths of each observational method. *INDEX TERMS:* 4594 Oceanography: Physical: Instruments and techniques; 4294 Oceanography: General: Instruments and techniques; 4275 Oceanography: General: Remote sensing and electromagnetic processes (0689); 0394 Atmospheric Composition and Structure: Instruments and techniques; *KEYWORDS:* sea surface temperature, VIRS SST, TMI SST

Citation: Ricciardulli, L., and F. J. Wentz (2004), Uncertainties in sea surface temperature retrievals from space: Comparison of microwave and infrared observations from TRMM, *J. Geophys. Res.*, *109*, C12013, doi:10.1029/2003JC002247.

1. Introduction

[2] Sea surface temperatures (SSTs) on a global scale have been successfully observed from space for the past 30 years. Advances in the technology in recent years greatly improved the performances of the satellite sensors observing the ocean temperatures. However, there are some scientific limitations to the accuracy of these observations, and they mostly lay in the uncertainties on the atmospheric attenuation of the radiation emitted by the ocean surface before it reaches the satellite sensors.

[3] Remote sensing of SSTs has traditionally been performed with sensors that operate in the infrared (IR) portion of the electromagnetic spectrum, where the ocean emissivity is close to unity. The Advanced Very High Resolution Radiometer (AVHRR) on NOAA satellites [*Cracknell*, 1997], the GOES Imagers on the Geostationary Operational Environmental Satellites [*Menzel and Purdom*, 1994], the Along Track Scanning Radiometer (ATSR) on the European Remote Sensing satellites [*Mutlow et al.*, 1994], and, recently, the Moderate Resolution Imaging Spectroradiometer (MODIS) on the NASA EOS platform [*Esaias et al.*, 1998] are successful examples of IR sensors currently used for operational SST retrievals. One great advantage of the IR ocean retrievals is the high spatial resolution (on the order of 1 km), which is very valuable in coastal waters and regions with strong thermal gradients. However, in the presence of clouds, IR sensors measure the cloud top temperature rather than the ocean surface temperature. Therefore SSTs are retrieved with IR only in clear-sky conditions, a significant limitation. Moreover, very extensive and complex cloud tests have to be performed on the IR radiances in order to minimize cloud-contaminated retrievals [*Saunders and Kriebel*, 1988; *Hutchison and Hardy*, 1995]. A major source of uncertainty in IR SST retrievals is the correction for water vapor attenuation. Most of the IR algorithms take into account atmospheric water vapor effects by measuring the difference in brightness temperature observed by two sensor channels, at slightly different IR frequencies but with significantly different water vapor absorption. Alternatively, some sensors (i.e., ATSR [*Zavody et al.*, 1995]) take advantage of the differential absorption at two different viewing angles as well as at two different channels.

0148-0227/04/2003JC002247$09.00

[4] In addition to the multichannel algorithms, there have been some attempts to incorporate measurements of atmospheric water vapor from other sensors in the IR algorithms [*Emery et al.*, 1994], in order to better estimate the atmospheric absorption of ocean-emitted radiation. A comprehensive review of the current IR algorithms for SST retrievals and their limitations is presented by *Barton* [1995]. In addition, a recent study by *Kumar et al.* [2003] investigates in depth the uncertainties of the atmospheric water vapor correction used in some IR algorithms for SST retrievals.

[5] Significant progress in SST remote sensing came with the introduction of a new low-frequency channel (10.7 GHz) on microwave (MW) sensors that allowed SST retrievals [*Wentz et al.*, 2000]. The great advantage of MW observations from space is that at lower frequencies, they are only slightly affected by water vapor and the effect can be removed. Therefore they provide an unprecedented view of the ocean surface through the clouds, with the only exception of rainy areas. However, MW SST retrievals are subject to other limitations, such as a lower spatial resolution (on the order of 50 km) due to limited size of the antenna on current satellites. Other sources of uncertainties are the variability of the ocean emissivity in the MW and its dependence on sea surface roughness. For this reason, MW SST retrievals might be biased in the presence of high winds.

[6] Sea surface temperatures have successfully been retrieved with the TRMM Microwave Imager (TMI) since 1997, and recently with the Advanced Microwave Scanning Radiometer (AMSR-E) on the NASA EOS AQUA platform [*Wentz et al.*, 2003]. The TRMM satellite provided the first opportunity to observe the ocean surface simultaneously with IR and MW sensors (Visible Infrared Scanner, VIRS, and TMI, respectively). We found this opportunity very valuable for investigating the characteristics of the uncertainties of each observational method and for studying in greater detail the water vapor effects on IR SST retrievals.

[7] Our analysis of the SST differences is also a prerequisite for the development of a new generation of SST data sets obtained by blending multisensor retrievals, one of the objectives of the Global Ocean Data Assimilation Experiment High-Resolution SST Pilot Project (GODAE-GHRSST-PP, http://www.ghrsst-pp.org). The combination of independent SST retrievals from in situ and space-based sensors using different methodology is one effective way to reduce the scientific limitations on SST retrievals and increase their accuracy. However, differences and error characteristics for each SST data set must be understood and taken into account for a successful blending process.

[8] In this paper, we describe an intercomparison of 1 year of SSTs obtained from the VIRS and TMI sensors. The two sensors are both on TRMM: They are colocated and observe the Earth in the same atmospheric conditions. We complemented the two SST data sets with an ancillary data set that includes colocated wind and water vapor retrievals from TMI and another estimate of SST interpolated from the weekly Reynolds OI data set. We then performed an intercomparison of VIRS and TMI SSTs and stratified the retrievals in terms of latitude, time of observation, atmospheric water vapor, wind, satellite viewing geometry, and proximity to land. In order to analyze the potential sources of error, we studied the IR/MW SST differences as a function of each of the variables listed above. In particular we investigated in detail the effects of water vapor and satellite viewing configuration on IR SST retrievals. In addition to some conventionally adopted multichannel IR algorithms, we tested the ability of some alternative forms of the multichannel algorithm to correct for water vapor effects. Finally, the coincident time of IR and MW observations from a non-Sun-synchronous orbit allowed a detailed comparison of the diurnal cycle of retrieved SSTs, which is significant in tropical regions in low winds conditions.

[9] We first start with a short description of TMI SST observations [*Wentz et al.*, 2000]. VIRS observations and our method for SST retrievals are described in section 3. Section 4 presents a brief description of the ancillary data sets used in our analyses. In section 5, we present a preliminary comparison of our VIRS SSTs versus VIRS daily maps provided by NASDA, the OI SSTs by Reynolds, and buoy SSTs. Section 6 is dedicated to the detailed investigation of error characteristics and uncertainties in both VIRS and TMI SSTs due to satellite maneuvers and viewing geometry, water vapor, wind, land contamination, aerosols, and undetected clouds. Finally, in section 7 we discuss some implications of our results on the choice of IR algorithm and possible methods to reduce errors in IR or MW SST retrievals from space. Appendix A lists the cloud detection tests performed on VIRS observations.

2. TMI Data

[10] The TRMM Microwave Imager TMI [*Kummerow et al.*, 1998] is a conical scanning radiometer with nine channels at five frequencies, ranging from 10.7 to 85.5 GHz. The instrument views the Earth with a 53° Earth incidence angle. Its rotating conical scanner records observations only during a 130° arc of the scanned circle, resulting in a 760-km swath width (increased to 880 km after orbit boost in 2001). The elliptical instantaneous field of view (IFOV) is frequency dependent. Microwave SSTs are determined from the 10.7-GHz channel, with an IFOV of approximately 65 × 35 km. Because of sampling overlap, the separation between adjacent observations is 13 km.

[11] TMI SSTs are routinely processed at Remote Sensing Systems (RSS) [*Wentz et al.*, 2000]. TMI ocean data are produced using a physically based algorithm developed from a radiative transfer model using simulated data. Reynolds SSTs are used to calibrate and remove biases from TMI brightness temperatures. Data within 100 km from land are excluded in the algorithm development, but the full range of wind observations is included. The algorithm for retrieving SSTs from MW observations is complicated and is thoroughly described by *Wentz and Meissner* [1999]. The TMI SST data, from December 1997 until present, are stored as 0.25° daily maps separately for ascending and descending passes and are available online at http://www.remss.com. TMI SSTs have been extensively validated [*Stammer et al.*, 2003; *Gentemann et al.*, 2004].

3. VIRS Data Preparation

[12] The Visible Infrared Scanner (VIRS) is a passive cross-track scanning radiometer on TRMM [*Kummerow et al.*, 1998; *Barnes et al.*, 2000]. Similarly to the AVHRR on the NOAA satellites, VIRS measures radiance in five

spectral bands, centered around 0.63, 1.61, 3.75, 10.8, and 12 μm, for channels 1 to 5, respectively. The Instantaneous Field of View (IFOV) is 2.11 km at nadir and the instrument scans a ±45° degree angle in 261 pixels, with a 720-km swath covering the tropics (38°N–38°S). The orbit altitude was moved from 360 km to 400 km in August 2001 to extend the mission lifetime, resulting in a wider swath, now 830 km. The analyses presented in this paper use 1 year of preboost data, from January to December 1998; in order to further confirm the validity of our conclusions, some of the analyses have been repeated using VIRS data for 1999, and are briefly mentioned in the next sections. We started from the level 1B product files, which were reprocessed at Remote Sensing Systems to reduce the size and to store reflectance and brightness temperatures instead of channel radiances. VIRS radiometric noise is lower than 0.1 K, allowing good quality SST retrievals.

[13] The main objective of VIRS visible and infrared observations is to observe the cloud top temperature to complement tropical rainfall observations from other sensors (precipitation radar and TMI). However, the same IR radiances can be used to retrieve the sea surface temperature. Daily maps of VIRS SSTs are produced and supplied by the Earth Observation Research Center of the National Space Development Agency (NASDA) of Japan. In order to colocate the VIRS observations with TMI, have the flexibility to test several IR algorithms, and then perform the analyses described in this paper, we processed VIRS brightness temperatures from the orbital files and created our own version of VIRS SSTs.

[14] The creation of a VIRS SST data set involved three major steps: the development of an efficient cloud detection algorithm able to select clear-sky observations, the use of an additional SST data set in order to calculate regression coefficients for the different forms of the SST algorithm, and finally the calculation of SSTs from VIRS brightness temperatures.

3.1. Cloud Detection Algorithm

[15] For an efficient detection of cloud-contaminated retrievals using VIRS visible and IR channels, we relied on the well-tested cloud mask developed for the AVHRR [*May et al.*, 1998]. The VIRS radiometer is very similar to AVHRR, with only slight differences in the spectral windows of each channel and a coarser spatial resolution (AVHRR resolution is 1.1 km at nadir). The cloud algorithm developed for AVHRR data can be easily modified to detect clouds with VIRS during nighttime, as only IR channels are involved. During the day, visible and near-IR channels are very helpful in cloud detection, since the cloud reflectivity is much higher than the ocean background. Generally, a simple threshold on reflectivity can discriminate cloud-contaminated observations. However, for particular Sun-satellite viewing angles, such as at high solar zenith angles or when the satellite is looking in the direction of specular reflection of solar radiation (Sun-glint), the ocean reflectivity is high even for clear sky and the simple reflectivity threshold method cannot be applied. Since TRMM is on a precessing quasi-equatorial orbit, the VIRS cloud mask needs to address a wide variety of Sun-satellite configurations, unlike the AVHRR that is on Sun-synchronous polar orbiters.

[16] In order to maximize the number of successful VIRS retrievals during daytime and avoid large areas of missing data due to Sun-glint (as large as 100 × 1000 km), we developed a method to adjust the reflectivity to normal conditions in these particular cases, allowing us to use the threshold method to discriminate clouds. Using 1 year (1998) of clear-sky VIRS data, we calculated an empirical adjustment to the reflectivity of channels 1 and 2 as a function of solar zenith angle, Sun-glint angle, and satellite scan angle. The empirical adjustment proved to be very efficient in allowing retrievals even in Sun-glint regions.

[17] In addition to daytime tests on the adjusted reflectivity, the cloud detection algorithm we applied to VIRS data is a suite of tests on spatial coherence, and on cirrus and low stratus cloud detection performed by comparing the brightness temperatures detected by pairs of IR channels, very similar to the AVHRR tests described by *May et al.* [1998], with some recently added enhanced (T_4-T_5) and cirrus tests (D. Olszewski, personal communication, 2002). We included an additional test with latitude-dependent thresholds to reject unrealistically cold SSTs, based on a similar test from *Schluessel and Albert* [2001] performed on brightness temperatures. The cloud detection tests are listed in detail in Appendix A.

3.2. VIRS SST Algorithms

[18] After applying the cloud mask, VIRS SSTs can be determined from the observed brightness temperatures using an empirically derived regression algorithm. Here we focus on the multichannel algorithms [*McMillin and Crosby*, 1984; *McClain et al.*, 1985], currently adopted for many operational SST products. These algorithms are based on the assumption that the brightness temperature observed by the satellite can be represented in terms of the surface temperature and an atmospheric correction term proportional to the difference between two channels, which represents an estimate of the atmospheric attenuation mostly due to water vapor. Several forms of the multichannel algorithms have been developed in recent years and are extensively described by *Barton* [1995], *Walton* [1988], *Emery et al.* [1994], and *Walton et al.* [1998]. One objective of our IR/MW intercomparison is to assess the ability of some of these algorithms to correct for atmospheric attenuation and satellite viewing configurations.

[19] In this study, we tested several forms of the dual (or split) and triple-window algorithm, and of the water vapor algorithms. The first is the nonlinear sea surface temperature algorithm (NLSST) (1a) for daytime retrievals, conventionally adopted for AVHRR retrievals by the Naval Oceanographic Office [*May et al.*, 1998; *Kilpatrick et al.*, 2001]. Another algorithm we considered (1b) is a linear daytime multichannel SST (MCSST), in a form like the one adopted by NASDA for their VIRS SSTs (H. Murakami, Sea surface temperature estimation using Visible and Infrared Scanner (VIRS), 1999, available at http://www.eorc.nasda.go.jp/TRMM/imgdt/day_vrs/virs_sst.pdf) [see also *Guan et al.*, 2003]. In addition, we considered two variations ((1c) and (1d)) of the water vapor algorithm WVSST introduced by *Emery et al.* [1994]: We assumed that the water vapor correction can be expressed as a linear term in water vapor W_V and an additional term weighted by the secant of the satellite zenith angle ϑ. For water vapor values in the algorithm, we used colocated and accurate observations

Table 1a. Coefficients for the VIRS SST Algorithms in Equations (1a)–(1d) (Daytime Retrievals) Determined by Regressing One Year (1998) of VIRS Brightness Temperatures to Colocated TMI SSTs

	a	b	c	d	e	f
NLSST	−239.49	0.88676	0.075109	0.51692	-	-
MCSST	−280.43	1.0248	2.1132	0.64058	-	-
WVSST1	−270.13	2.6105	−1.6212	0.035511	0.053702	-
WVSST2	−179.33	−3.0558	3.7421	0.1940	0.0044071	0.040234

made with the TRMM Microwave Imager (TMI). These observations were not available before 1998; in their WVSST algorithm for AVHRR retrievals, *Emery et al.* [1994] used water vapor estimates from the Special Sensor Microwave Imager SSMI [*Schluessel and Emery*, 1990] colocated on a timescale of 2 days.

$$NLSST = a + bT_4 + c(T_4 - T_5)SST_{fg} + d(T_4 - T_5)F_\vartheta, \quad (1a)$$

$$MCSST = a + bT_4 + c(T_4 - T_5) + d(T_4 - T_5)F_\vartheta, \quad (1b)$$

$$WVSST_1 = a + bT_4 + cT_5 + d \cdot W_V + e \cdot W_V F_\vartheta, \quad (1c)$$

$$WVSST_2 = a + bT_4 + cT_5 + d(T_4 - T_5)SST_{fg} + e \cdot W_V + f \cdot W_V F_\vartheta. \quad (1d)$$

[20] Here, T_4, and T_5 are the brightness temperatures observed by VIRS channel 4 and 5, respectively; SST_{fg} is a first guess SST (in our case from TMI), ϑ is the satellite zenith angle; $F_\vartheta = \sec(\vartheta) - 1$; a, b, c, d, e, and f are coefficients to be estimated by regression for each algorithm; and W_V is the colocated water vapor from TMI. Owing to solar contamination at 3.75 μm, channel 3 is not considered in the daytime algorithms. Night algorithms ((2a)–(2d)) are slightly different as they also include brightness temperatures T_3 from the near-IR channel 3.

$$NLSST = a + bT_4 + c(T_3 - T_5)SST_{fg} + d \cdot F_\vartheta, \quad (2a)$$

$$MCSST = a + bT_4 + c(T_4 - T_5) + d(T_4 - T_5)F_\vartheta + e(T_3 - T_5) + f(T_3 - T_5)F_\vartheta, \quad (2b)$$

$$WVSST_1 = a + bT_3 + cT_4 + dT_5 + e \cdot W_V + f \cdot W_V F_\vartheta, \quad (2c)$$

$$WVSST_2 = a + bT_3 + cT_4 + dT_5 + e(T_3 - T_5)SST_{fg} + f \cdot W_V + g \cdot W_V F_\vartheta. \quad (2d)$$

3.3. Creation of VIRS SST Data Sets

[21] The coefficients a, b, c, d, e, f, and g in (1a)–(1d) and (2a)–(2d) were estimated by regressing cloud-free VIRS brightness temperatures to 1 year (1998) of colocated TMI SSTs, separately for day and night and for each algorithm, and are listed in Tables 1a and 1b. TMI data in the presence of wind speeds greater than 12 m/s were excluded from the regression in order to avoid potential biases in the microwave SST retrievals due to high winds. TMI SSTs different by more than 3°C from Reynolds SSTs were also excluded. Cloud-free retrievals used for the regression were determined performing the cloud tests on VIRS brightness temperatures and reflectivities listed in Appendix A. A set of orbital VIRS SSTs for the year 1998 was created from more than 900 million matches for each tested algorithm, at a spatial resolution of approximately 4 km. The orbital data were then gridded onto daily 0.125° × 0.125° tropical maps (from 1 January until 31 December 1998).

[22] For our comparisons, we colocated TMI with VIRS SSTs by determining which of the TMI 25 km grid boxes included the center of each 4 km × 4 km VIRS SST retrieval. No spatial averaging was performed, and the VIRS and TMI observations are nearly simultaneous. The colocated TMI retrievals were then stored in 0.125° maps, as the VIRS SSTs. In addition to TMI SSTs, we colocated other geophysical variables from TMI [*Wentz*, 1997] needed for our investigation: water vapor, 10-m wind speed, and time of observation.

[23] In order to include an independent data set in the analyses and to confirm that our approach is justified, we produced an alternative SST data set, the $VIRS_{Rey}$. In this case, new regression coefficients for the four VIRS algorithms were determined by regressing VIRS brightness temperatures to 1 year (1998) of weekly 100 km Reynolds SSTs instead of TMI SSTs. The change in SST data set used for the regression did not have a significant impact on the coefficients. Tables 2a and 2b show the coefficients for the $VIRS_{Rey}$ algorithms. The first-guess SST in the $VIRS_{Rey}$ algorithms was still represented by colocated TMI observations. Unless otherwise noted, the analyses presented in this paper refer to VIRS SSTs for 1998 determined by regression to TMI SSTs (coefficients in Tables 1a and 1b). VIRS SSTs for 1999, using the coefficients in Tables 1a and 1b, were also analyzed as an additional proof of general validity of our conclusions; they will be briefly mentioned in the text in the next sections.

4. Other Ancillary Data Sets

[24] In addition to the TMI colocated variables, we stored 0.125° daily maps of SSTs interpolated from the 1° resolution weekly maps of Reynolds Optimal Interpolated (OI) SSTs developed at the National Center for Environmental Prediction [*Reynolds and Smith*, 1994; *Reynolds et al.*,

Table 1b. Same as Table 1a, but for Nighttime Retrievals (Equations (2a)–(2d))

	a	b	c	d	e	f	g
NLSST	−244.13	0.90728	0.03013	1.6320	-	-	-
MCSST	−262.22	0.97044	−1.0243	1.8592	1.2433	−0.57917	-
WVSST1	−255.81	0.98296	0.096845	−0.13259	0.031523	0.058693	-
WVSST2	−223.23	−0.93496	0.47015	1.3028	0.060316	0.020994	0.054312

Table 2a. Coefficients for the VIRS SST Algorithms in Equations (1a)–(1d) (Daytime Retrievals) Determined by Regressing One Year (1998) of VIRS Brightness Temperature to Reynolds SSTs

	a	b	c	d	e	f
$NLSST_{Rey}$	−237.62	0.88093	0.070943	0.65296	-	-
$MCSST_{Rey}$	−275.39	1.0079	2.0501	0.73038	-	-
$WVSST1_{Rey}$	−262.41	2.3823	−1.4191	0.045507	0.06169	-
$WVSST2_{Rey}$	−208.26	0.95505	1.7374	0.11443	0.027399	0.053526

2002]. For validation purposes, we obtained the VIRS SSTs processed by the Earth Observation Research Center, National Space Development Agency (NASDA) of Japan. The NASDA SSTs are supplied as daily maps on a 0.125° × 0.125° grid from 21 December 1997 until present. Observations from moored open-ocean buoys were included in our validation of VIRS SSTs. Buoy observations were collected from three sources, the U.S. National Data Buoy Center (NDBC), the Marine Environmental Data Service (MEDS, within Canada's Federal Department of Fisheries and Oceans), and the Pacific Marine Environmental Laboratory/NOAA.

5. VIRS SSTs Comparison With Other Data Sets

[25] Daily maps of VIRS SSTs derived using the four algorithms described above were compared to daily colocated TMI SSTs, the Reynolds daily interpolated OI SSTs, and the VIRS SST daily maps provided by NASDA, showing general agreement. Figures 1a–1c show the daily maps for a sample day (11 August 1998) for the VIRS SSTs determined with the NLSST algorithm (Figure 1a), the corresponding NASDA VIRS SSTs (Figure 1b), and the colocated TMI SSTs (Figure 1c). Figures 1a and 1b show that a significant portion of SST retrievals is missing because of cloud contamination. The two data sets (Figures 1a and 1b) are produced independently from the same VIRS IR radiances (not exactly the same brightness temperatures, as NASDA uses a central wavelength approximation for the spectral windows), but use different cloud detection and SST algorithms. Despite the different processing methods, our VIRS SSTs and NASDA SSTs are qualitatively very similar, with minor differences in the distribution of cloud contaminated areas, and small strips of missing data due to Sun-glint conditions in the central Pacific (west of Hawaii) in the NASDA retrievals. Figure 1c shows the TMI retrievals only in cloud-free areas, to facilitate the comparison with VIRS SSTs.

[26] When compared to TMI observations for all of 1998, VIRS SSTs did not show any significant bias. This was expected since the VIRS SST algorithm coefficients were regressed using TMI SSTs. The very small negative bias (−0.1°C) found for all the tested VIRS algorithms can be attributed to the more stringent conditions applied in the regression process to VIRS brightness temperatures and colocated TMI observations in order to exclude potentially cloud contaminated pixels and high wind retrievals. The average standard deviation (Table 3) of daily differences between VIRS and TMI SSTs is on the order of 0.7°C, with slightly lower values for the VIRS algorithms that include the "first-guess" SST. For most of the algorithms, the standard deviation is lower for night retrievals because of the use of the additional VIRS channel 3. Similar results were found comparing $VIRS_{Rey}$ SSTs to TMI.

[27] Comparison of VIRS SSTs with Reynolds OI SSTs also did not show any bias for 1998 data. An average standard deviation of 0.7°C was found when comparing daily VIRS maps versus daily-interpolated Reynolds SSTs. A similar value was found for the standard deviation of daily TMI SSTs versus daily-interpolated Reynolds SSTs. Finally, we compared our VIRS SSTs to daily maps of VIRS SST provided by NASDA. In this case the standard deviation was 0.45°C, without bias. When compared to Reynolds SSTs, NASDA SSTs for 1998 show a standard deviation of 0.78°C, without bias.

[28] A comparison of daily VIRS SSTs and moored buoys for 1998 showed a small negative bias (−0.1°C) and an average standard deviation between 0.55°C and 0.60°C, for the four tested algorithms. The colocated TMI SSTs showed a similar bias and a 0.45°C standard deviation compared to buoys, consistent with *Gentemann et al.* [2004].

[29] Overall, the use of Reynolds coefficients (Tables 2a and 2b) did not have a major impact on the VIRS SSTs. The average standard deviation of daily differences between $VIRS_{Rey}$ and VIRS SSTs used for the analyses presented in this paper (for 1998) is 0.12°C, with a small bias (0.04°C).

[30] Despite the general similarities in VIRS and TMI SSTs, some major differences among the data sets emerge when we take a closer look. As an example, Figure 2 shows the differences between VIRS NLSST and TMI SSTs or VIRS and Reynolds SSTs, averaged over a month (for January and July 1998). Compared to TMI, VIRS NLSSTs in January (Figure 2a) have a warm bias in the equatorial regions. The geographical distribution of the warm SST bias is well correlated with regions of high atmospheric water vapor (i.e., see TMI monthly water vapor maps at http://www.remss.com/tmi). While water vapor has the effect of decreasing the brightness temperature observed by the

Table 2b. Same as Table 2a, but for Nighttime Retrievals (Equations (2a)–(2d))

	a	b	c	d	e	f	g
$NLSST_{Rey}$	−243.49	0.90496	0.03000	1.8108	-	-	-
$MCSST_{Rey}$	−260.96	0.96566	−0.96341	1.9386	1.2353	−0.58603	-
$WVSST1_{Rey}$	−255.42	1.0088	0.21820	−0.28131	0.021071	0.060715	-
$WVSST2_{Rey}$	−245.37	0.44411	0.33067	0.13714	0.017442	0.019364	0.059589

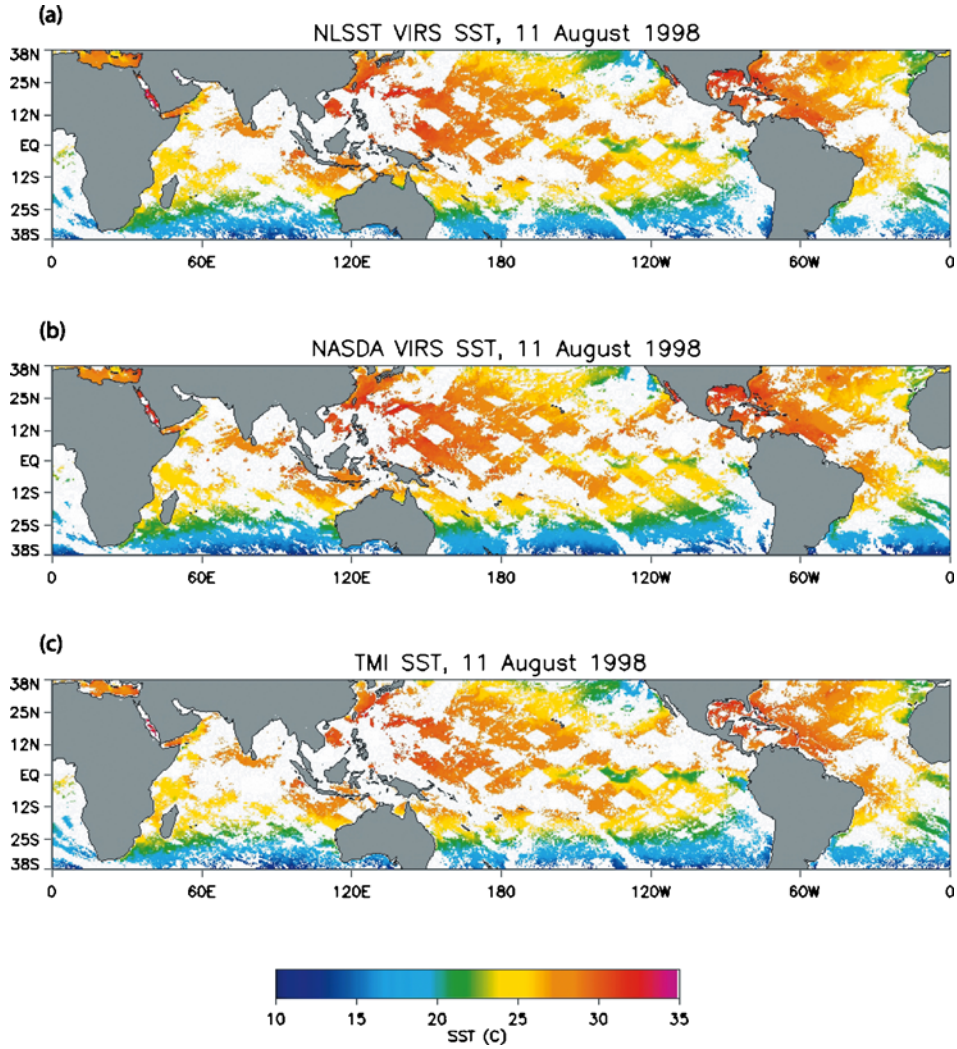

Figure 1. Daily sea surface temperature maps (0.125° resolution) for 11 August 1998, for the VIRS SSTs determined with (a) the NLSST algorithm, (b) the NASDA SSTs, and (c) the colocated (clear-sky) TMI SSTs.

sensor at infrared frequencies, resulting in cold biased SSTs, here the warm bias is likely due to an overcorrection for high water vapor in the NLSST algorithm, and will be discussed in more detail in section 6.3. Also evident in Figure 2a is a region with large SST differences in the North Pacific, at the edge of the satellite swath. In July (Figure 2c), the average VIRS-TMI shows a cold bias west of Africa, likely due to contamination from Saharan dust aerosols (see section 6.7), and a positive SST difference in the eastern Pacific region at the equator affected by tropical instability waves. Figures 2b and 2d show the average VIRS(NLSST)-Reynolds SST, where small-scale geophysical features and areas of strong thermal gradients (i.e., Gulf stream and loop current, Kuroshio current, and Agulhas current) are not sufficiently resolved in the Reynolds data compared to VIRS.

6. Analysis of Uncertainties in SST Retrievals

[31] Despite the small average bias for VIRS data compared to TMI or OI Reynolds SSTs, temporal variations in a 0.5°C range do occur, as shown in Figure 3a. The figure shows daily differences of NLSST-TMI; the time series was extended to include also VIRS data from 1999 in order to investigate potential year-to-year changes or satellite drifts. The gray vertical lines in Figure 3 are placed to denote a yaw change in the TRMM satellite, and suggest that greater differences between VIRS and TMI SSTs are found soon after changing yaw. They are possibly the result of change in the thermal environment of the instruments (TRMM performs yaw maneuvers approximately every month to avoid excessive solar heating of the instruments). The time series of VIRS-TMI also shows a variation with a cycle of approximately 40 to 50 days, which might be due to a "diurnal cycle" of the TRMM sensors, which observe the Earth at a different local time for each day, precessing every 46 days. Figure 3b shows the temporal variation of the VIRS-TMI standard deviation, which reaches a maximum during the boreal summer, likely due to the increased amount of aerosols in this season which might affect the IR SST retrievals, as discussed in a separate section (see section 6.7).

[32] In order to understand the sources of errors and uncertainties in both IR and MW retrievals, we stratified the VIRS, TMI, and Reynolds daily SSTs in terms of water

Table 3. Standard Deviation of SST Differences for One Year of Gridded Maps at 0.125° Resolution (1998), for the Average Daily Retrievals and for Daytime or Nighttime Retrievals Separately

	Daily Standard deviation (°C)	Daytime standard deviation (°C)	Nighttime standard deviation (°C)
NLSST-TMI	0.71	0.72	0.70
MCSST-TMI	0.77	0.80	0.73
$WVSST_1$-TMI	0.77	0.79	0.75
$WVSST_2$-TMI	0.68	0.67	0.70
NLSST-Reynolds	0.71	0.74	0.68
TMI-Reynolds	0.70	0.72	0.69

vapor, wind speed, latitude, time of observation, and satellite angle. In the following paragraphs we discuss each effect separately.

6.1. Satellite Viewing Geometry

[33] As already mentioned, the VIRS instrument scans a ±45° angle in 261 pixels. The increased path length at high satellite zenith angles ϑ results in greater attenuation of IR radiation by water vapor and other atmospheric constituents. The brightness temperatures observed at the edge of the scan are colder than those observed at the center of the scan, and the difference depends on the satellite angle ϑ, the sensor's channel wavelength, and the water vapor column in the observed regions. For VIRS channels 5 (Figure 4), the brightness temperature T_5 at the edge of the scan is about 2 K colder than the temperature at the center of the scan for water vapor $20 < W_V < 50$ mm. For this reason, all the SSTs algorithms (equations (1a)–(1d) and (2a)–(2d)) include the term $F_\vartheta = \sec(\vartheta) - 1$ to correct for increased path length at high satellite viewing angles. Despite the corrective term, some residual dependence on scan angle ϑ is still evident and affects the SST retrievals. Figure 5 shows the average SST difference VIRS-TMI for 1998 as a function of the scan position, for three regimes of water vapor and for two of the tested algorithms. The NLSST algorithm (Figure 5a) reveals a significant dependence on satellite viewing angle

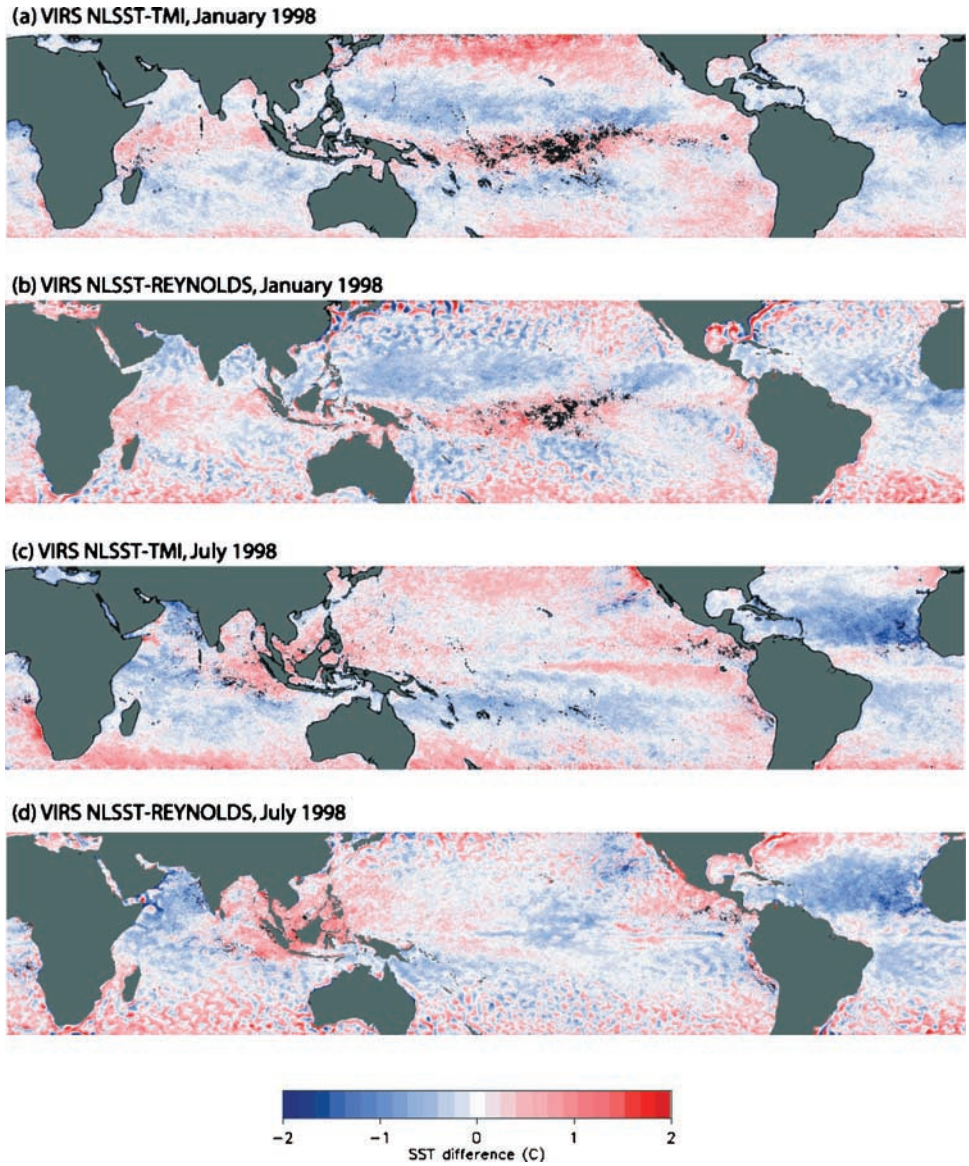

Figure 2. Monthly (a, c) VIRS(NLSST)-TMI and (b, d) VIRS(NLSST)-Reynolds SST differences for January 1998 (Figures 2a and 2b, respectively), and July 1998 (Figures 2c and 2d, respectively).

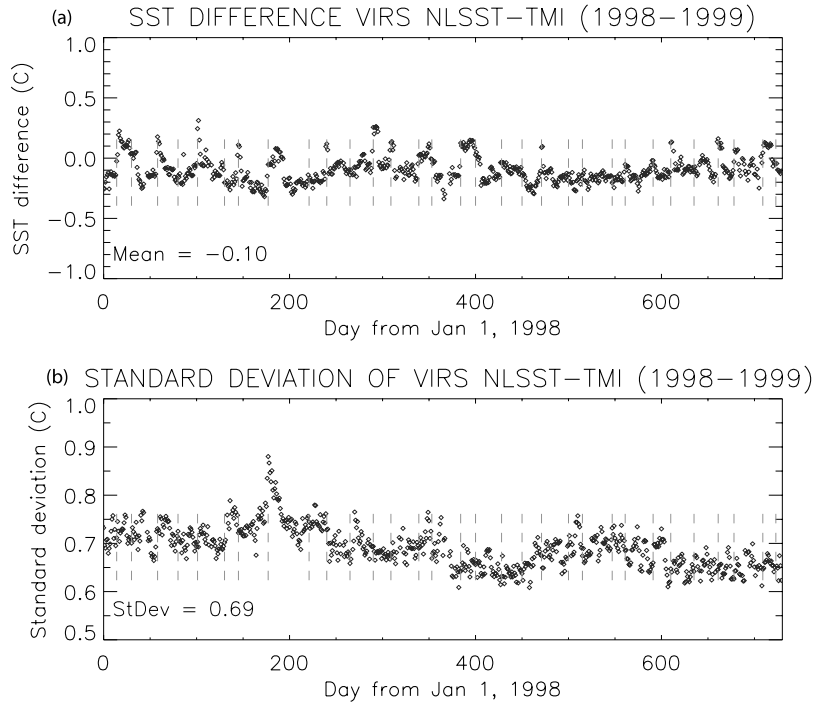

Figure 3. (a) Difference between daily VIRS(NLSST) and the colocated TMI SSTs for 1998 and 1999. The vertical dashed lines refer to a change in satellite yaw. (b) The corresponding standard deviation about the daily mean difference.

when the atmosphere has a high water vapor content (greater than 50 mm), with SSTs at the edge up to 0.4°C colder than those retrieved at the center of the scan. Figure 5b shows the average SST difference for the water vapor algorithm $WVSST_1$-TMI. Because of the inclusion of W_V in the algorithm weighted by the F_ϑ term, these SSTs are less affected by scan angle, except for low water vapor atmospheric conditions, where the corrective term does not seem to be efficient. The investigation of satellite viewing geometry effects was repeated with the 1998 $VIRS_{Rey}$ SSTs, and did not show significant differences compared to Figure 5, except for increased biases at high and low water vapor with the $WVSST_1$ algorithm.

6.2. Water Vapor

[34] To correct for atmospheric water vapor effects, the multichannel SST algorithms rely on the differential absorption by a pair of thermal channels (i, j), represented by the term $(T_i - T_j)$. In order to be able to express the SST algorithm in the multichannel form, a number of assumptions are made [*Walton et al.*, 1998]. However, some of the assumptions might not be valid under all atmospheric conditions, for example for high atmospheric absorption [see *Walton*, 1988; *Barton*, 1995].

[35] The efficiency of these algorithms in estimating atmospheric attenuation was questioned by *Emery et al.* [1994], who suggested alternative forms including a quadratic term in $(T_i - T_j)$ or explicit water vapor in the SST algorithms. Here we analyze the residual dependence of each algorithm's SSTs on atmospheric water vapor. In Figure 6, we show the difference between VIRS and TMI SSTs averaged over 1 year for each algorithm, for daily averages (Figure 6a) and daytime retrievals only (Figure 6b). As discussed, water vapor affects only VIRS retrievals, while microwaves at 10.7 GHz are only weakly sensitive to it. Without the correction for atmospheric water vapor, the VIRS-TMI difference would have a negative bias at high water vapor. Figure 6a illustrates that the NLSSTs, where the brightness temperature channel difference is weighted by a first-guess SST, have a residual warm bias (~0.3°C) at high and low water vapor, possibly the effect of an overcorrection by the nonlinear term.

[36] This effect is also visible in Figure 5a, where the VIRS NLSST-TMI differences for high and low water vapor observed at the center of the scan are warmer than those at

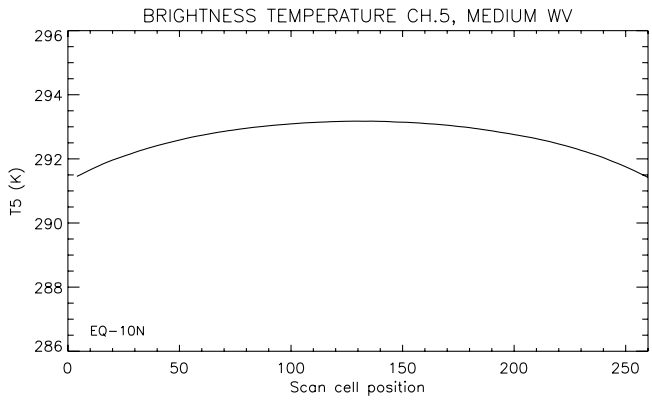

Figure 4. Observed brightness temperature for VIRS channel 5 as a function of scan position. Data from the region between the equator and 10°N for medium water vapor conditions ($20 < W_V < 50$ mm) were averaged for all 1998.

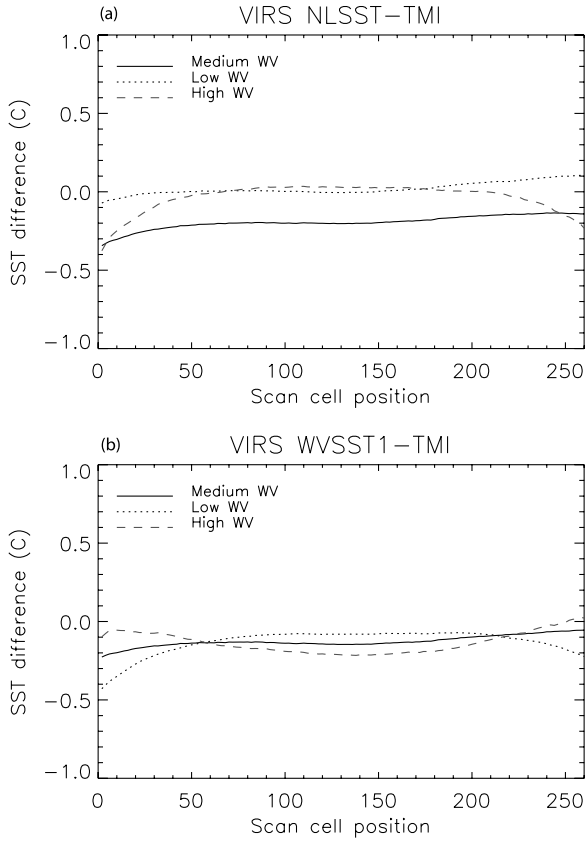

Figure 5. VIRS-TMI SSTs as a function of the satellite scan cell position for three water vapor regimes: low ($10 < W_V < 20$ mm), medium ($30 < W_V < 40$ mm), and high ($50 < W_V < 60$ mm). The SST differences are averages for 1 year of data (1998), for two of the tested algorithms, (a) the NLSST and (b) the $WVSST_1$.

medium water vapor. The simpler MCSSTs have a minor residual dependence on water vapor with a very small cold bias for water vapor >50 mm. Interestingly, the bias affects mostly nighttime retrievals (not shown) with the NLSST, and day time retrievals (Figure 6b) with the MCSST. When water vapor is explicitly considered in the algorithm $WVSST_1$, the VIRS SSTs do not show significant residual water vapor effects. In the figure, SST differences obtained with an alternative water vapor algorithm $WVSST_2$, which includes water vapor weighted by a first guess SST, are also shown. These retrievals show a significant dependence on water vapor. However, the bad performance of this algorithm is masked by a lower standard deviation of $WVSST_2$-TMI (see Table 3), which in this case is not a good indicator of decreased error in the VIRS retrievals. One important feature to look at in Figure 6 is the curvature of the bias, a function of water vapor, which for $WVSST_2$ would result in regional biases in dry or moist regions.

[37] *Kumar et al.* [2003] found a large negative SST bias for high water vapor conditions in the Arabian Sea, using the Pathfinder algorithm and SSMI water vapor. However, at midlatitudes they found a tendency for the algorithm to overcorrect for water vapor. The Pathfinder algorithm is the NLSST with only two channels for both night and day retrievals (channels 4 and 5, like the daytime algorithm (1a)) and Reynolds SSTs as first guess. Regression coefficients are determined versus buoys (with different coefficients for different latitude bands). The comparison with our results is not straightforward. Our study does not focus on regional biases. However, if we look only at the 38°N–38°S average daytime VIRS NLSST-TMI versus water vapor (Figure 6b), there is no bias, except for a small positive bias at low water vapor. The nighttime NLSST algorithm is responsible for the overcorrection at high water vapor in the average daily VIRS observations. From this perspective, our results do not contradict those of *Kumar et al.* [2003].

[38] The conclusions drawn in the previous paragraph are based on the assumption that TMI SSTs are not affected by water vapor. This is the result of both physical reasons and processing operations. Microwaves at 10.7 GHz, used to retrieve TMI SSTs, are only weakly sensitive to water vapor; any residual effect is removed from TMI retrievals by using higher frequency channels. Figure 7 shows that compared to buoys or Reynolds SSTs, TMI SSTs for 1998 are free of water vapor biases. In addition, Figure 8 presents the difference between VIRS and buoy SSTs (1998) for each algorithm, leading to results similar to those in Figure 6a. Note that there are only approximately 6000 match-ups with buoys in 1998, with few or no matches at low and high water vapor conditions. On the other hand, VIRS-TMI has millions of matches in 1 year, making the

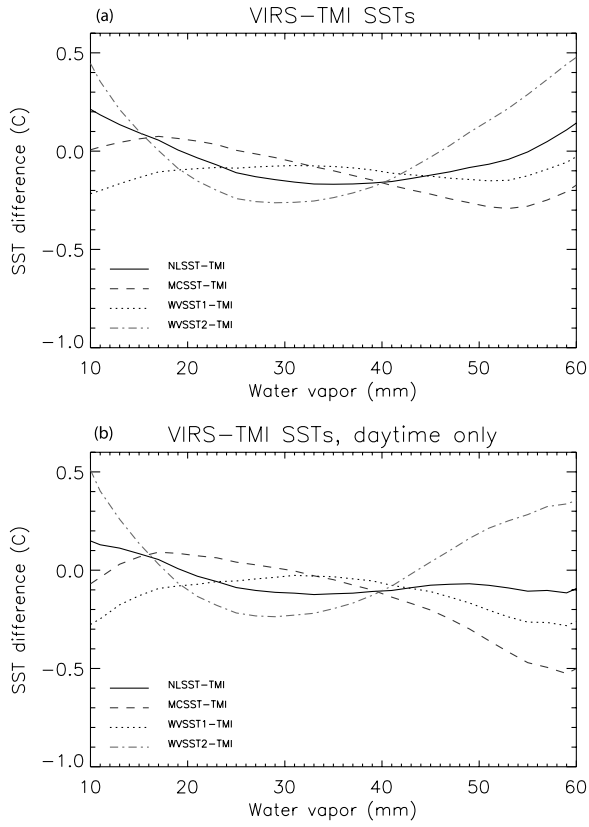

Figure 6. VIRS-TMI SSTs as a function of the atmospheric water vapor column. The SST differences are averages for 1 year of data (1998), for the four tested algorithms: NLSST, MCSST, $WVSST_1$, and $WVSST_2$. (a) Combined daytime + nighttime retrievals. (b) Daytime only retrievals.

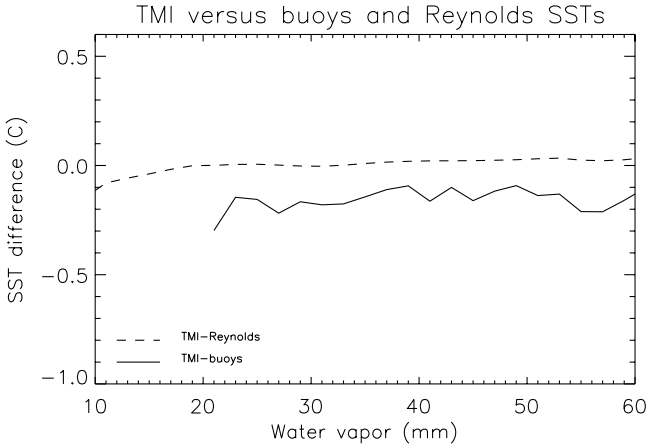

Figure 7. TMI-Reynolds SSTs and TMI-buoy SSTs as a function of water vapor, for the combined nighttime + daytime retrievals for the entire 1998.

results more statistically significant. To further validate these results, we repeated the analysis of water vapor biases in Figure 6 using the VIRS SST data set for 1999 and the $VIRS_{Rey}$ data set for 1998. The VIRS-TMI differences for these alternative VIRS data sets (not shown) are very similar to those in Figure 6. One notable difference was found for the $WVSST_2$ algorithm using the Reynolds coefficients, which showed reduced warm biases at low and high water vapor compared to Figure 6a, with maximum biases of the order of 0.2°–0.3°C. The results presented in this section include retrievals for all wind conditions: Performing the analysis only with retrievals corresponding to moderate winds (between 5 and 12 m/s; not shown) did not alter the results.

6.3. Surface Winds

[39] The ocean emissivity in the microwave spectrum is very sensitive to the surface wind speeds that alter the sea roughness [*Hollinger*, 1971; *Wentz*, 1975]. For this reason, MW SST algorithms take into account different wind regimes, in order to minimize wind effects on SST retrievals [*Wentz and Meissner*, 1999]. In the infrared spectrum, *Harris et al.* [1994] hypothesized the presence of some wind effects, and found that a decrease in IR emissivity for windy ocean (wind speed > 15 m/s) could lead to errors in retrieved SSTs up to 0.4°C for a dry atmosphere, but has small effects in the tropical atmosphere. More recent studies [*Watts et al.*, 1996; *Wu and Smith*, 1997; *Henderson et al.*, 2003] included the effects of reflection of radiation emitted by a wind-roughened sea surface in their models and found that these effects almost compensate the reduction of emissivity at high winds. *Watts et al.* [1996] estimated that the assumptions of constant (zero-wind speed) emissivity and specular reflection have a very small net effect on brightness temperatures (or SST), on the order of 0.1 K.

[40] In order to study the effects of winds on MW and IR SST retrievals, we analyzed the differences between VIRS or TMI SSTs and the daily-interpolated Reynolds SSTs, as a function of surface wind speed. Figure 9 shows VIRS-Reynolds SSTs for the NLSST algorithm. Except for low winds, VIRS SSTs do not seem to be affected by wind speed, both in terms of bias and standard deviation (in Figure 10). At wind speeds less than 5 m/s, the VIRS SSTs during the day are warmer than the Reynolds SSTs, as expected because of the effects of the diurnal warming of the ocean skin layer.

[41] The differences between TMI and Reynolds SSTs are illustrated in Figure 11, as a function of wind speed. As the MW algorithm implicitly accounts for surface wind speed, on the average TMI SSTs do not show any bias due to wind effects. However, at high wind speeds we notice a significant increase in the standard deviation (Figure 10). Therefore, even if not biased, TMI SSTs at high wind speeds have a much greater uncertainty. At low wind speeds, TMI SSTs show the effects of diurnal warming, similar to VIRS SSTs. However, TMI SSTs seem to have a cold bias at night for low wind speed, due to an apparent nocturnal cooling, not seen in VIRS SSTs. The effects of diurnal warming/nocturnal cooling on SSTs are discussed in detail in the next paragraph.

6.4. Diurnal Cycle of SSTs

[42] Infrared sensors observe the ocean skin temperature at a depth of few microns, while microwaves measure the subskin temperatures at a depth of approximately 1 mm [*Wentz et al.*, 2000]. Both the skin and subskin layers are subject to a diurnal warming due to solar radiation.

[43] The availability of multiyear data sets of in situ and satellite observations of the ocean temperatures led to detailed investigations about the thermal properties of the upper ocean, the diurnal cycle, and the difference between skin and bulk SST [*Fairall et al.*, 1996; *Webster et al.*, 1996; *Wick et al.*, 1996; *Donlon and Robinson*, 1997; *Emery et al.*, 2001; *Donlon et al.*, 2002; *Wick et al.*, 2002; *Gentemann et al.*, 2003]. Here we briefly analyze the diurnal signal in VIRS SSTs and compare it to the one in TMI SSTs.

[44] In general terms, the amplitude of the diurnal warming depends on the daily insolation and time of the day, on the measurement depth, and on the surface wind speed. For winds greater than about 5 to 7 m/s, the upper ocean is well mixed and solar heating is distributed throughout the upper 2–100 m of the ocean. In order to analyze the diurnal signal in VIRS and TMI SST retrievals, we compared them to the daily-interpolated Reynolds SSTs, and stratified the data in

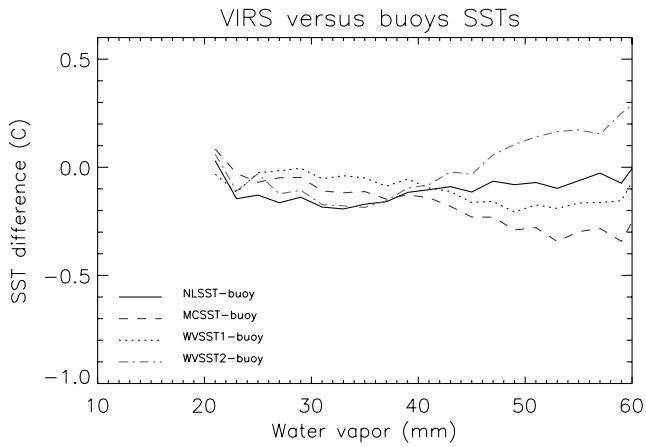

Figure 8. Average daily differences between VIRS and buoy SSTs for 1998, as a function of water vapor.

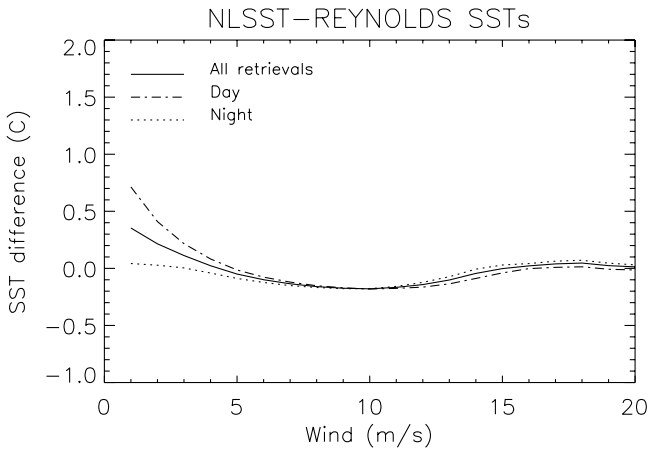

Figure 9. VIRS(NLSST)-Reynolds daily interpolated SSTs, for 1998 data. The figure shows the average difference for all retrievals (solid line) as a function of surface wind speed. Also shown are day (dash-dotted line) and night retrievals (dotted line).

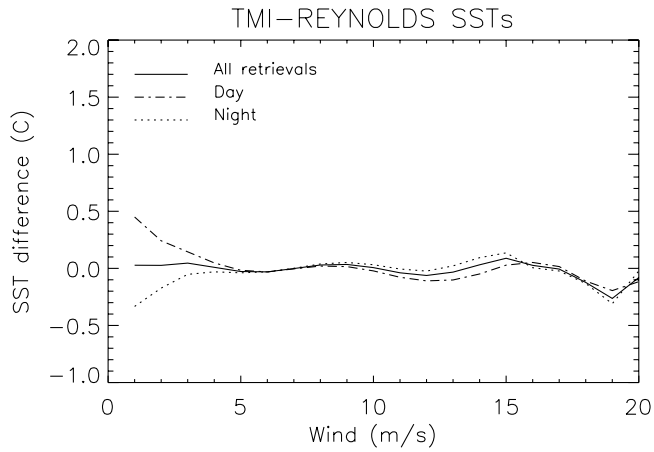

Figure 11. Same as Figure 9, but for clear-sky TMI-Reynolds SSTs.

terms of local time of observation, for all retrievals or only for low winds. The Reynolds SSTs do not contain any major diurnal signal as they are interpolated from weekly data and they represent an ocean bulk temperature, corresponding to approximately 1 m depth. A weak heating due to inclusion of daytime AVHRR data in the Reynolds SST product might be present, but the effect has not been estimated.

[45] In Figure 12 we show the difference between VIRS (NLSST) and Reynolds SSTs as a function of the local time of the day, for 1 year of data in all wind conditions, and for low winds only (less than 3 m/s). A significant diurnal variability is evident for the VIRS SSTs in low winds, as a result of the solar warming of the upper ocean layer (centimeters). The average amplitude of the diurnal signal is on the order of 1°C, with a peak value at about 1400 LT, and slowly decaying even after the local midnight. The minimum temperatures are found in the early morning hours, at about 0600 LT. The effect of the diurnal warming is not present for higher winds, and the average difference

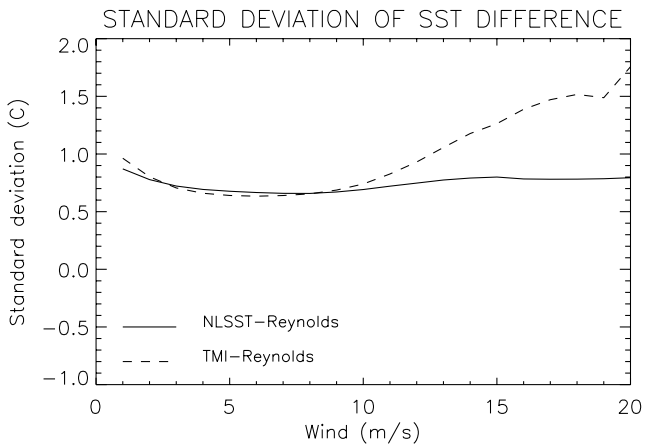

Figure 10. Standard deviation of SST differences for VIRS(NLSST)-Reynolds (solid line) and TMI-Reynolds (dashed line) for 1998, as a function of wind speed.

VIRS-Reynolds SST for retrievals in all wind conditions (or for moderate winds between 5 and 12 m/s, not shown) is approximately constant throughout the day. Similar results about the diurnal warming were found for the other three VIRS tested algorithms.

[46] The difference between TMI and Reynolds SSTs in Figure 13 highlights a similar diurnal signal for TMI at low winds, consistent with previous studies [*Gentemann et al.*, 2003]. One major difference between VIRS and TMI diurnal cycle is an apparent nocturnal cooling in the TMI SSTs at low winds, which could be a geophysical feature or an artifact of the processing operations on TMI data. As already mentioned, TMI SSTs are determined using a physically based ocean product algorithm and then corrected for biases. A zero bias was imposed to TMI SSTs for all winds. Therefore, the positive bias due to diurnal warming at low wind speeds is compensated by a negative bias at night (see Figure 11, section 6.3). While the magnitude of the nocturnal cold bias in TMI SSTs is likely an artifact of data processing, its existence is supported by theoretical and observational studies, which predict a cool skin at night, with skin temperatures approximately 0.2°–0.3°C colder than bulk SSTs [*Fairall et al.*, 1996; *Donlon et al.*, 2002; *Wick et al.*, 2002]. Our analysis of VIRS SSTs (which are not subject to any wind bias correction) does not show nocturnal cooling, for reasons yet to be determined. The difference between the diurnal cycle of VIRS and TMI SSTs, explicitly presented in Figure 14, ranges between 0.3°C (day) and 0.5°C (night) at low winds, and suggests a slightly larger diurnal warming of the skin temperature compared to the subskin.

6.5. Land Contamination

[47] At microwave frequencies, land surfaces have a higher emissivity (0.9) compared to the ocean (0.4). Microwave observations in the proximity of land are affected by the warm emission of land entering the antenna near-in sidelobes. This warming of the microwave brightness temperatures is a source of errors in the TMI retrievals of coastal waters. Since infrared retrievals are not affected by land emission (if retrieved at least a few kilometers from the coast), the difference between TMI and VIRS SSTs is a

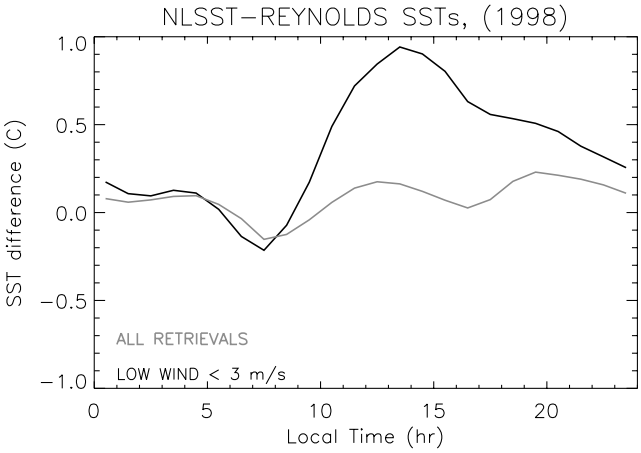

Figure 12. VIRS NLSST-Reynolds daily-interpolated SSTs as a function of the local time of the day. The differences are averaged over 1 year of data (1998), for all retrievals (shaded line) and in low wind conditions only (black line). The lines refer to the average between ascending and descending orbit retrievals, in order to avoid time averaging.

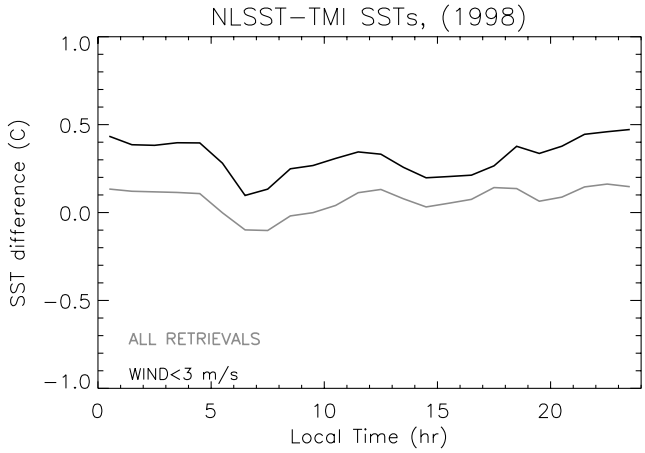

Figure 14. Same as Figure 13, but for VIRS NLSST-TMI SSTs.

good indicator of the bias of TMI SSTs due to land contamination. Figures 15a and 15b show differences between TMI and VIRS (NLSST) SSTs for two sample regions, Africa and Hawaii, averaged over 1 month (January 1998). The land contamination produces a systematic warm bias of TMI SSTs on the order of 1°C in regions within 50–100 km from land.

6.6. Undetected Clouds

[48] Cloud detection is a very critical step in SST retrievals from infrared observations. *May et al.* [1998] and *Kilpatrick et al.* [2001] provide extensive description of cloud detection algorithms for AVHRR. While most of the cloud-contaminated observations are easily detected with tests on spatial coherence of brightness temperatures and on differential absorption by a pair of thermal channels, some clouds are very difficult to detect (i.e., broken clouds, optically thin clouds, cirrus and low stratus clouds). In many cases, after applying the cloud detection algorithm and determining the SSTs, a further test is applied which rejects all the retrievals that are 2° or 3°C colder than other independently estimated SSTs (like the weekly Reynolds SSTs). However, this test might not be sufficient to screen warm low clouds, or it might result in rejection of good retrievals in coastal waters or in areas with strong currents, since the weekly Reynolds SSTs do not have the spatial and temporal resolution to observe highly variable geophysical features. The availability of simultaneous observations with microwave techniques provides a good opportunity to estimate residual undetected clouds in the VIRS SST products. As an example, Figure 16 shows the difference of VIRS-TMI SSTs for 4 January 1998. The light gray areas correspond to regions where SST retrievals are not available for that day because they were not sampled by TRMM or were flagged as cloud contaminated in the VIRS data. The figure clearly highlights some regions with significant cold bias in VIRS SSTs, on the order of 2°C or more. Since these regions are in the proximity of patchy cloud-contaminated areas, it is very likely they are also cloud contaminated but were not flagged by the tests in the cloud detection algorithm.

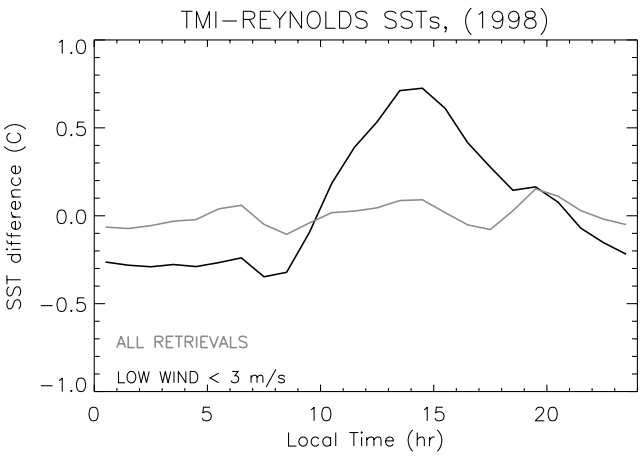

Figure 13. Same as Figure 12, but for TMI-daily interpolated Reynolds SSTs.

6.7. Aerosols

[49] Atmospheric aerosols represent another factor that results in a possible cold bias in SSTs determined from IR observation, as they increase the atmospheric attenuation of IR radiation detected by the satellite sensor. Potential aerosols contamination in VIRS SSTs requires an extensive investigation that was not the main objective of the study presented in this paper. However, as it represents a major source of errors and uncertainties in SST retrievals from IR sensors, we briefly address it.

[50] A detailed study of tropospheric aerosols over the ocean [*Husar et al.*, 1997] showed the existence of areas of persistent high optical depth associated with wind-blown dust and biomass burning sources, particularly west of Africa, in the Middle East and in South Asia. Husar et al. identified a seasonal variability of the distribution of tropo-

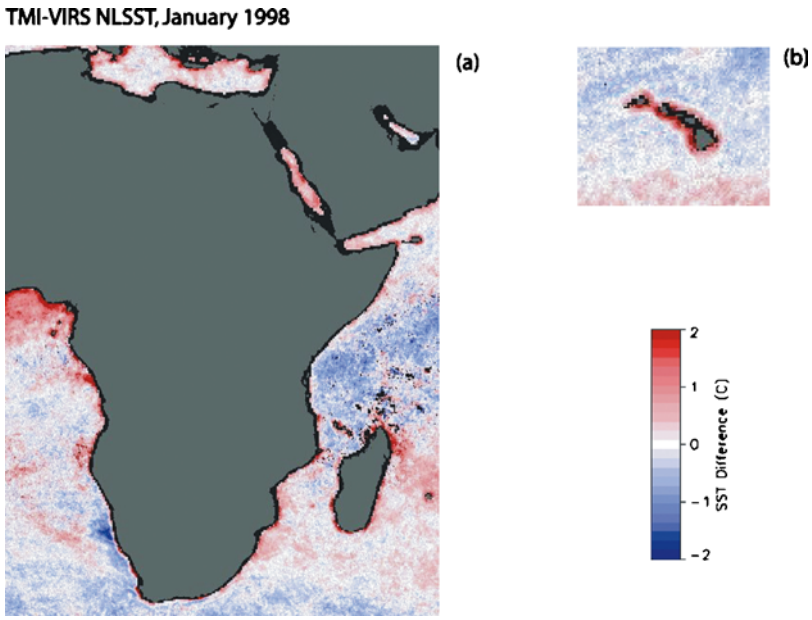

Figure 15. Map of monthly average SST difference between TMI and VIRS NLSST, for January 1998, for (a) Africa and (b) the coastal waters of Hawaii, showing warm biased TMI SSTs due to land contamination.

spheric aerosols, with highest values in the Northern Hemisphere summer and minimum in winter [i.e., *Husar et al.*, 1997, Plates 1 and 2]. In addition, aerosols of volcanic origin can affect IR SST retrievals on a global scale for several months following an eruption [*Reynolds*, 1993].

[51] Since microwave radiation is not affected by the presence of atmospheric aerosols, a comparison of VIRS-TMI SSTs might emphasize aerosol-contaminated regions in the VIRS retrievals. As an example, Figure 2c shows the average difference between VIRS (NLSST) and TMI SSTs for July 1998. Compared to the same difference in January 1998 (Figure 2a), in July we notice a persistent area of colder VIRS SSTs west of Africa and in the Arabian Sea, located in regions of high aerosols optical depth. Figure 2c shows that if not properly screened by the cloud mask, some aerosols can lead to significant cold bias in IR SST retrievals, on the order of 1°C or more. This result is consistent with other studies, which attribute a cold bias to satellite retrieved SSTs in the presence of dust aerosols [*Diaz et al.*, 2001; *Zhang et al.*, 2004].

7. Discussion and Conclusions

[52] We performed a detailed intercomparison of 1 year (1998) of SSTs observed simultaneously by the infrared VIRS and microwave TMI sensors on the TRMM satellite. The analyses presented here are aimed at understanding the error characteristics of SST retrievals from infrared and microwave observations, and at developing strategies to minimize errors and uncertainties.

[53] We investigated in detail the effects of water vapor and satellite viewing angle on IR SSTs retrievals, and tested the performance of a number of algorithms. We found that despite the corrective terms in the IR SST algorithms, some residual dependence on atmospheric water vapor and path length can still lead to biases on the order of a few tenths of

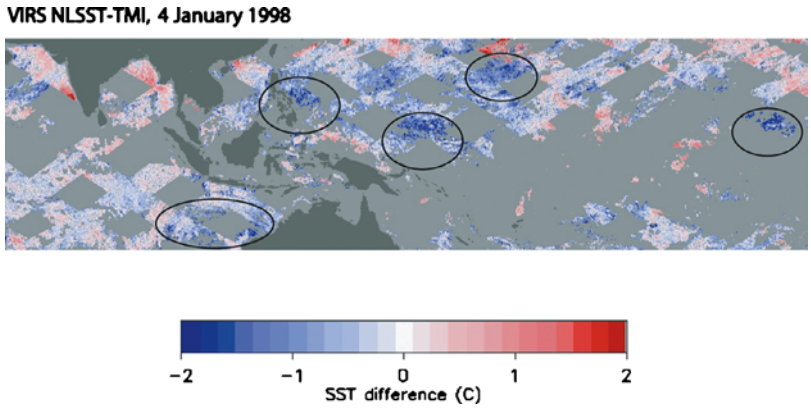

Figure 16. Map of daily average SST difference between VIRS(NLSST) and TMI, for 4 January 1998. Some areas of potential contamination by undetected clouds in the VIRS SSTs are circled.

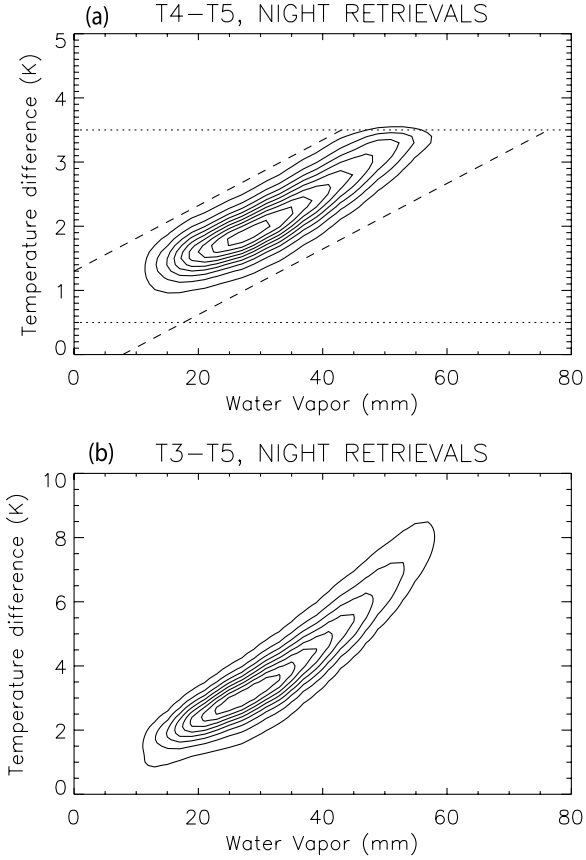

Figure 17. Probability distribution function (PDF) of brightness temperature channel difference versus water vapor for 1 year of ungridded VIRS observations averaged over a 4 × 4 km box. Night retrievals of (a) (T_4-T_5) and (b) (T_3-T_5). The PDFs are normalized and contours are linear. The dotted lines in Figure 17a refer to the range of validity of clear-sky retrievals in most of the current algorithms. The dashed lines refer to a proposed cloud test to detect clear-sky IR observations using colocated MW observations of water vapor.

a degree. The inclusion of a linear term in water vapor in the algorithm reduces these biases, except for retrievals in very dry atmospheric conditions. However, this type of water vapor SST algorithm can only be used when accurate and simultaneous observations of water vapor are available.

[54] On the other hand, microwave observations are highly sensitive to surface winds. The MW algorithm implicitly corrects for wind biases, but our comparison between VIRS and TMI SSTs showed a higher uncertainty associated with TMI SST retrievals for winds greater than 12 m/s. The proximity to land also affects MW SSTs, resulting in a warm bias on the order of 1°C within 50–100 km from land. The comparison between VIRS and TMI SSTs as a function of latitude (not shown) did not show any significant bias, except for a warm bias (∼0.4°C) and higher standard deviation (∼1.2°C) at extratropical latitudes, at the edge of the TRMM orbital swath. The standard deviation of the VIRS(NLSST)-TMI SST difference of daily 0.125° maps is 0.7°C, but it reduces to 0.66°C when the difference is performed using lower resolution maps, obtained with a 5 × 5 pixels moving average. This result implies that most of the differences between VIRS and TMI SSTs are not attributed to differences in the sensors' sampling resolution. In addition, the use of a land mask in TMI data extended to 100 km from the coast does not have a significant impact on the standard deviation between VIRS and TMI SSTs.

[55] Both VIRS and TMI SSTs were used to investigate the amplitude of the diurnal variation of skin and subskin temperatures. A significant diurnal warming was found for both data sets in the presence of low winds, consistent with other extensive studies. It is important to note that the diurnal cycle in TMI and VIRS is a real geophysical signal, not to be confused with an uncertainty in the data. However, data users need to be aware of this signal when they compare these data to ocean bulk temperature, like those from buoys or the Reynolds OI SSTs. The aim of this investigation is not to determine which SST algorithm is overall superior to the others, but rather to provide the users with alternative metrics to evaluate the performance of the algorithms, beyond the global standard deviation, and choose the optimal algorithm for their application.

[56] These results showed that both infrared and microwave observation of the ocean temperature can benefit from their comparison. For example, the comparison of SSTs obtained from of a number of IR algorithms with other independent SST observations (TMI, Reynolds OI or buoys) can help identify the optimal IR algorithm in terms of accuracy. On the other hand, SST differences between TMI and VIRS highlighted the need for a modification of the land mask in TMI SST retrievals in order to minimize warm bias due to land contamination.

[57] After the major reasons for differences between VIRS and TMI SSTs are excluded (high winds, diurnal signal, water vapor, etc.), the residual differences might be due to undetected clouds or aerosols in infrared retrievals. Currently, most of the cloud detection algorithms apply a constant threshold (or one dependent on brightness temperature) to channel differences (T_i-T_j) to discriminate clear-sky observations: All retrievals outside a specified range (typically between 0.5 K and 3.5 K for (T_4-T_5) and between 0.5 K and 8 K for (T_3-T_5), respectively) are flagged as cloud contaminated. In reality, these differences are highly dependent on the atmospheric conditions. As an example, in Figure 17 we show the probability distribution function (PDF) of 1 year of observed brightness temperature differences between pairs of channels, as a function of atmospheric water vapor. The figure shows that the channel differences for clear-sky retrievals are limited by different values for different water vapor regimes. These PDFs could be used to design an improved physically based cloud test for which the range of clear-sky IR retrievals is a function of colocated MW water vapor (dashed lines in Figure 17a) rather than a constant value (dotted lines) valid for all atmospheric regimes.

[58] One of the main motivations for this study was the need to quantify differences and uncertainties in IR/MW SST retrievals in order to combine them and produce a blended IR/MW SST data set, such as the one under development under the coordination of the GODAE HRSST project. This data set takes advantage of each method's strength, but cannot be performed with a blind eye with respect to differences due to the observational method. The

Table A1. VIRS Cloud Tests Parameters

Test	Parameters
Daytime Tests	
Gross cloud test on T_4	$270\ K < T_4 < 310\ K$
Gross cloud test on T_5	$268\ K < T_5 < 310\ K$
Near IR uniformity, channel 2 adjusted reflectivity	$\max(R_2)_{ij} - \min(R_2)_{ij} < 0.02$
IR uniformity, T_4	$\max(T_4)_{ij} - \min(T_4)_{ij} < 1\ K$
IR uniformity, T_5	$\max(T_5)_{ij} - \min(T_5)_{ij} < 1\ K$
Enhanced (T_4-T_5) test	$0 < T_4\text{-}T_5 < \min(0.005604 \times T_4^2 - 3.03079 \times T_4 + 411.45\ K, 3.5\ K)$
Visible test, channel 1 adjusted reflectivity	$R_1 < 0.08$
Near IR test, channel 2 adjusted reflectivity	$R_2 < 0.06$
Nighttime Tests	
Gross cloud test on T_3	$270\ K < T_3 < 310\ K$
Gross cloud test on T_4	$270\ K < T_4 < 310\ K$
Gross cloud test on T_5	$268\ K < T_5 < 310\ K$
IR uniformity, T_3	$\max(T_3)_{ij} - \min(T_3)_{ij} < 1\ K$
IR uniformity, T_4	$\max(T_4)_{ij} - \min(T_4)_{ij} < 1\ K$
IR uniformity, T_5	$\max(T_5)_{ij} - \min(T_5)_{ij} < 1\ K$
Enhanced (T_4-T_5) test	$0 < T_4\text{-}T_5 < \min(0.005604 \times T_4^2 - 3.03079 \times T_4 + 411.45\ K, 3.5\ K)$
Enhanced stratus/cirrus test	if $T_4 > 292\ K$ then $0 < (T_3\text{-}T_5)/T_5 < 0.033\ K$; otherwise, $0 < (T_3\text{-}T_5)/T_5 < \exp(0.004191 \times T_4^2 - 2.293899 \times T_4 + 309.042032)$

intercomparison of IR/MW SSTs will have the additional benefit of providing users with an estimate of the uncertainties associated to each SST data set, valuable information for short-range forecast or climate modelers. In the future, we plan to perform similar intercomparisons with AMSR-E and MODIS SSTs, observed by the AQUA EOS platform.

Appendix A: Cloud Tests

[59] The VIRS cloud tests are performed on 2 × 2 pixel arrays (approximately 4 km × 4 km). R_1, R_2, T_3, T_4, and T_5 are the 2 × 2 average reflectivity for channels 1 and 2, and brightness temperatures for channels 3, 4, and 5, respectively; $(T_3)_{i,j}$, $(T_4)_{i,j}$ $(T_5)_{i,j}$ are the brightness temperature for each (i, j) pixel in the 2 × 2 array box, with i,j = 1,2. The daytime tests (solar zenith angle SZA < 88°) are performed after adjusting the reflectivity of channels 1 and 2 for satellite-Sun geometry effects. Test details are given in Table A1.

[60] If the brightness temperature and reflectivities pass all these tests, the SSTs are determined using the algorithms described in section 3.2. Then, the VIRS SSTs (in °C) are subject to additional screening by using latitude-dependent thresholds and by comparing them to other SST retrievals:

$$\text{VIRS SST} > 17 \times \cos(\text{lat} \times \text{acos}(9/17)/40),$$

$$|\text{VIRS SST - TMI SST}| < 3°\text{C},$$

$$|\text{VIRS SST - Reynolds SST}| < 3°\text{C},$$

where lat is the average latitude for the 2 × 2 pixel array.

[61] In the regression process, after performing the cloud screening on brightness temperatures and reflectivity, a first-guess set of VIRS SSTs was determined for each 2 × 2 array using some preliminary regression coefficients. The first-guess VIRS SSTs for the four algorithms (k = 1, 2, 3, 4) listed in section 3.2 were then subject to the following additional screening:

$$\max(\text{VIRS SST})_{k=1,2,3,4} > 17 \times \cos(\text{lat} \times \text{acos}(9/17)/40),$$

$$|\text{average}(\text{VIRS SST})_{k=1,2,3,4} - \text{TMI SST}| < 3°\text{C},$$

$$|\text{average}(\text{VIRS SST})_{k=1,2,3,4} - \text{Reynolds SST}| < 3°\text{C}.$$

[62] **Acknowledgments.** This work was accomplished at Remote Sensing Systems and supported by NASA contract NAS5-00217 and JPL-1228578. Frances Bergmann at NASA Goddard Space Flight Center DAAC kindly provided the VIRS level-1B01 data, which were kindly copied to tapes by Bill Teng at the GSFC DAAC. Chelle Gentemann at Remote Sensing Systems reprocessed the VIRS level-1B data to store brightness temperatures instead of radiances and to reduce the size of the files. The NASDA version of VIRS data VIRSSST (version 1.0), used in some of the comparisons with RSS VIRS SSTs, was produced and supplied by the Earth Observation Research Center, National Space Development Agency of Japan. The authors are very grateful to Douglas May, Bruce McKenzie, and Daniel Olszewski for helpful discussions about the AVHRR cloud mask. The manuscript benefited from thorough reviews and valuable comments from two anonymous reviewers.

References

Barnes, R. A., W. L. Barnes, C.-H. Lyu, and J. M. Gales (2000), An overview of the visible and infrared scanner radiometric calibration algorithm, *J. Atmos. Oceanic Technol.*, *17*, 395–405.

Barton, I. J. (1995), Satellite-derived sea surface temperature: Current status, *J. Geophys. Res.*, *100*, 8777–8790.

Cracknell, A. P. (1997), *The Advanced Very High Resolution Radiometer (AVHRR)*, 534 pp., Taylor and Francis, Philadelphia, Pa.

Diaz, J. P., M. Sarbelo, F. J. Exposito, G. Podestá, J. M. Prospero, and R. Evans (2001), Relationship between errors in AVHRR-derived sea surface temperature and the TOMS Aerosol Index, *Geophys. Res. Lett.*, *28*, 1989–1992.

Donlon, C. J., and I. S. Robinson (1997), Observations of the oceanic thermal skin in the Atlantic Ocean, *J. Geophys. Res.*, *102*, 18,585–18,606.

Donlon, C. J., P. J. Minnett, C. L. Gentemann, T. J. Nightingale, I. J. Barton, B. Ward, and M. J. Murray (2002), Toward improved validation of satellite sea surface skin temperature measurements for climate research, *J. Clim.*, *15*, 353–369.

Emery, W. J., Y. Yu, G. A. Wick, P. Schluessel, and R. W. Reynolds (1994), Correcting infrared satellite estimates of sea surface temperature for atmospheric water vapor attenuation, *J. Geophys. Res.*, *99*, 5219–5236.

Emery, W. J., S. Castro, G. A. Wick, P. Schluessel, and C. Donlon (2001), Estimating sea surface temperature from infrared satellite and in situ temperature data, *Bull. Am. Meteorol. Soc.*, *82*, 2773–2785.

Esaias, W. J., et al. (1998), An overview of MODIS capabilities for ocean science observations, *IEEE Trans. Geosci. Remote Sens.*, *36*, 1250–1265.

Fairall, C. W., E. F. Bradley, J. S. Godfrey, G. A. Wick, J. B. Edson, and G. S. Young (1996), Cool skin and warm layer effects on sea surface temperature, *J. Geophys. Res.*, *101*, 1295–1308.

Gentemann, C. L., C. J. Donlon, A. Stuart-Menteth, and F. J. Wentz (2003), Diurnal signals in satellite sea surface temperature measurements, *Geophys. Res. Lett.*, *30*(3), 1140, doi:10.1029/2002GL016291.

Gentemann, C. L., F. J. Wentz, C. A. Mears, and D. K. Smith (2004), In situ validation of Tropical Rainfall Measuring Mission microwave sea surface temperatures, *J. Geophys. Res.*, *109*, C04021, doi:10.1029/2003JC002092.

Guan, L., H. Kawamura, and H. Murakami (2003), Retrieval of sea surface temperature from TRMM VIRS, *J. Oceanogr.*, *59*, 245–249.

Harris, A. R., S. J. Brown, and I. M. Mason (1994), The effect of wind speed on sea surface retrieval from space, *Geophys. Res. Lett.*, *21*, 1715–1718.

Henderson, B. G., J. Theiler, and P. Villeneuve (2003), The polarized emissivity of a wind-roughened sea surface: A Monte Carlo model, *Remote Sens. Environ.*, *88*, 453–467.

Hollinger, J. P. (1971), Passive microwave measurements of sea surface roughness, *IEEE Trans. Geosci. Electron.*, *9*(3), 165–169.

Husar, R. B., J. M. Prospero, and L. L. Stowe (1997), Characterization of tropospheric aerosols over oceans with the NOAA advanced very high resolution radiometer optical thickness operational product, *J. Geophys. Res.*, *102*, 16,899–16,909.

Hutchison, K. D., and K. R. Hardy (1995), Threshold functions for automated cloud analyses of global meteorological satellite imagery, *Int. J. Remote Sens.*, *16*, 3665–3680.

Kilpatrick, K. A., G. P. Podestá, and R. H. Evans (2001), Overview of the NOAA/NASA advanced very high resolution radiometer Pathfinder algorithm for sea surface temperature and associated matchup database, *J. Geophys. Res.*, *106*, 9179–9197.

Kumar, A., P. J. Minnett, G. Podestá, and R. H. Evans (2003), Error characteristics of the atmospheric correction algorithms used in retrievals of sea surface temperatures from infrared satellite measurements: Global and regional aspects, *J. Atmos. Sci.*, *60*, 575–585.

Kummerow, C., W. Barnes, T. Kozu, J. Shiue, and J. Simpson (1998), Tropical Rainfall Measuring Mission (TRMM) Sensor Package, *J. Atmos. Oceanic Technol.*, *15*, 809–817.

May, D. A., M. M. Parmeter, D. S. Olszewski, and B. D. McKenzie (1998), Operational processing of satellite sea surface temperature retrievals at the Naval Oceanographic Office, *Bull. Am. Meteorol. Soc.*, *79*, 397–407.

McClain, E. P., W. G. Pichel, and C. C. Walton (1985), Comparative performance of AVHRR-based multichannel sea surface temperatures, *J. Geophys. Res.*, *90*, 11,587–11,601.

McMillin, L., and D. Crosby (1984), Theory and validation of the multiple window sea surface temperature technique, *J. Geophys. Res.*, *89*, 3655–3661.

Menzel, W. P., and J. F. Purdom (1994), Introducing GOES-1: The first of a new generation of geostationary operational environmental satellites, *Bull. Am. Meteorol. Soc.*, *75*, 757–781.

Mutlow, C. T., A. M. Zavody, I. J. Barton, and D. T. Llewellyn-Jones (1994), Sea surface temperature measurements by the along-track scanning radiometer on the ERS 1 satellite: Early results, *J. Geophys. Res.*, *99*, 22,575–22,588.

Reynolds, R. W. (1993), Impact of Mount Pinatubo aerosols on satellite-derived sea surface temperatures, *J. Clim.*, *6*, 768–774.

Reynolds, R. W., and T. M. Smith (1994), Improved global sea surface temperature analyses using optimum interpolation, *J. Clim.*, *7*, 929–948.

Reynolds, R. W., N. A. Rayner, T. M. Smith, D. C. Stokes, and W. Wang (2002), An improved in situ and satellite analysis for climate, *J. Clim.*, *15*, 1609–1625.

Saunders, R. W., and K. T. Kriebel (1988), An improved method for detecting clear sky and cloud radiances from AVHRR data, *Int. J. Remote Sens.*, *9*, 123–150.

Schluessel, P., and A. Albert (2001), Latent heat flux at the sea surface retrieved from combined TMI and VIRS measurements of TRMM, *Int. J. Remote Sens.*, *22*, 1975–1998.

Schluessel, P., and W. J. Emery (1990), Atmospheric water vapor over oceans from the SSM/I measurements, *Int. J. Remote Sens.*, *11*, 753–766.

Stammer, D., F. Wentz, and C. Gentemann (2003), Validation of microwave sea surface temperature measurements for climate purposes, *J. Clim.*, *16*, 73–87.

Walton, C. C. (1988), Nonlinear multichannel algorithm for estimating sea surface temperature with AVHRR satellite data, *J. Appl. Meteorol.*, *27*, 115–124.

Walton, C. C., W. G. Pichel, J. F. Sapper, and D. A. May (1998), The development and operational application of nonlinear algorithms for the measurements of the sea surface temperatures with the NOAA polar-orbiting environmental satellites, *J. Geophys. Res.*, *103*, 27,999–28,012.

Watts, P. D., M. R. Allen, and T. J. Nightingale (1996), Wind speed effects on sea surface emission and reflection for the Along Track Scanning Radiometer, *J. Atmos. Oceanic Technol.*, *13*, 126–141.

Webster, P. J., C. A. Clayson, and J. A. Curry (1996), Clouds, radiation, and the diurnal cycle of sea surface temperature in the tropical western Pacific, *J. Clim.*, *9*, 1712–1730.

Wentz, F. J. (1975), A two-scale scattering model for foam-free sea microwave brightness temperatures, *J. Geophys. Res.*, *80*, 3441–3446.

Wentz, F. J. (1997), A well calibrated ocean algorithm for special sensor microwave imager, *J. Geophys. Res.*, *102*, 8703–8718.

Wentz, F. J., and T. Meissner (1999), AMSR Ocean Algorithm, version 2, *RSS Tech. Rep. 121599A*, 65 pp., Remote Sens. Syst., Santa Rosa, Calif. (Available at http://www.remss.com/support/publications.html)

Wentz, F. J., C. L. Gentemann, D. Smith, and D. Chelton (2000), Satellite measurements of sea surface temperature through clouds, *Science*, *288*, 847–850.

Wentz, F. J., C. Gentemann, and P. Ashcroft (2003), On-orbit calibration of AMSR-E and the retrievals of ocean products, paper presented at 83rd AMS Annual Meeting, Am. Meteorol. Soc., Long Beach, Calif.

Wick, G. A., W. J. Emery, L. H. Kantha, and P. Schluessel (1996), The behavior of the bulk-skin temperature difference under varying wind speed and heat flux, *J. Phys. Oceanogr.*, *26*, 1969–1988.

Wick, G. A., J. J. Bates, and D. J. Scott (2002), Satellite and skin-layer effects on the accuracy of the sea surface temperature measurements from the GOES satellites, *J. Atmos. Oceanic Technol.*, *19*, 1834–1848.

Wu, X., and W. L. Smith (1997), Emissivity of rough sea surface for 8–13 micron: Model and verification, *Appl. Opt.*, *36*, 2609–2619.

Zavody, A. M., C. T. Mutlow, and D. T. Llewelyn-Jones (1995), A radiative transfer model for sea surface temperature retrieval for along-track scanning radiometer, *J. Geophys. Res.*, *100*, 937–952.

Zhang, H.-M., R. W. Reynolds, and T. M. Smith (2004), Bias characteristics in the AVHRR sea surface temperature, *Geophys. Res. Lett.*, *31*, L01307, doi:10.1029/2003GL018804.

L. Ricciardulli and F. J. Wentz, Remote Sensing Systems, 438 First Street, Suite 200, Santa Rosa, CA 95401, USA. (ricciardulli@remss.com)